1972

Phenomenology based upon the generalized Veneziano model

David Edwin Johnson
Iowa State University

INFORMATION TO USERS

This dissertation was produced from a microfilm copy of the original document. While the most advanced technological means to photograph and reproduce this document have been used, the quality is heavily dependent upon the quality of the original submitted.

The following explanation of techniques is provided to help you understand markings or patterns which may appear on this reproduction.

1. The sign or "target" for pages apparently lacking from the document photographed is "Missing Page(s)". If it was possible to obtain the missing page(s) or section, they are spliced into the film along with adjacent pages. This may have necessitated cutting thru an image and duplicating adjacent pages to insure you complete continuity.

2. When an image on the film is obliterated with a large round black mark, it is an indication that the photographer suspected that the copy may have moved during exposure and thus cause a blurred image. You will find a good image of the page in the adjacent frame.

3. When a map, drawing or chart, etc., was part of the material being photographed the photographer followed a definite method in "sectioning" the material. It is customary to begin photoing at the upper left hand corner of a large sheet and to continue photoing from left to right in equal sections with a small overlap. If necessary, sectioning is continued again – beginning below the first row and continuing on until complete.

4. The majority of users indicate that the textual content is of greatest value, however, a somewhat higher quality reproduction could be made from "photographs" if essential to the understanding of the dissertation. Silver prints of "photographs" may be ordered at additional charge by writing the Order Department, giving the catalog number, title, author and specific pages you wish reproduced.

University Microfilms

300 North Zeeb Road
Ann Arbor, Michigan 48106

A Xerox Education Company

Phenomenology based upon the generalized Veneziano model

by

David Edwin Johnson

A Dissertation Submitted to the

Graduate Faculty in Partial Fulfillment of

The Requirements for the Degree of

DOCTOR OF PHILOSOPHY

Department: Physics
Major: High Energy

Approved:

Signature was redacted for privacy.

In Charge of Major Work

Signature was redacted for privacy.

For the Major Department

Signature was redacted for privacy.

For the Graduate College

Iowa State University
Ames, Iowa

1972

TABLE OF CONTENTS

ABSTRACT

This study is made of the reactions $\bar{p}p \rightarrow \bar{p}p\pi^{o}$, $\bar{p}n\pi^{+}$, and $p\bar{n}\pi^{-}$ at 2.9 GeV/c using a model which combines Pomeron diffraction-dissociation diagrams with generalized Beneziano model diagrams. Three model parameterizations, which differ in their relative amounts of Pomeron and dual amplitudes allowed, are examined for the $\bar{p}p\pi^{o}$ final state, and all are found to be in good agreement with the data. It is impossible to obtain a reasonable fit for the $\bar{p}n\pi^{+}$ and $p\bar{n}\pi^{-}$ final states with this model.

1. INTRODUCTION

In the few years since its conception, the Veneziano model[1] of incorporating duality[2] into the calculation of high energy scattering cross sections has appeared frequently in the literature.[3] This model has been applied to almost all of the two-body final state reactions and has been able to fit the data remarkably well.[4] With the extension of the Veneziano model to many-body final states,[5] three-body final state reactions were examined and were also found to be well represented by this formulation.[6] Only a limited class of three-body final state reactions has been calculated using the Veneziano model, because of the difficulty of applying the model to reactions in which the Pomeron Regge trajectory contributes.[7] In a recent paper a method was suggested by which the Pomeron trajectory contributions to a scattering process might be included in a Veneziano model calculation of a three-body reaction.[8] The purpose of this paper is to further examine such a composite model and to use it to study the general reaction $\bar{N}N \to \bar{N}N\pi$.

In Sec. II we give a description of the way the composite model is formed in order to include both Pomeron and dual contributions. In Sec. III we look at the particular final state $\bar{p}p \to \bar{p}p\pi^o$, determine the exact form of the composite parts of our model for this final state, and ascertain which of the possible dual diagrams must be considered. Three different parameterizations for the scattering cross section are constructed in which we make different assumptions about the details of the model. In Sec. IV is shown the results of applying each of these models

to the reaction $\bar{p}p \to \bar{p}p\pi^o$. In Sec. V the two remaining final states $\bar{p}p \to \bar{p}n\pi^+$, $p\bar{n}\pi^-$ are treated. Sec. VI is a brief discussion of the ability of this composite model to fit the three final states.

II. DESCRIPTION OF THE MODEL

Before one is able to study the general reaction $\bar{N}N \to \bar{N}N\pi$ using the Veneziano model, one must first determine a reasonable method with which to treat Pomeron scattering effects and include them in an overall scattering amplitude. Since an outgoing pion-nucleon system can form a state which has the same quantum numbers as the incoming nucleon, it is clear that processes involving the Pomeron trajectory must be considered in any treatment of this reaction. Pomeron exchange may not, however, be directly incorporate into a simple dual amplitude as the Pomeron trajectory cannot have any possible dual partner; that is, Pomeron exchange in one channel cannot be related to resonance production in any other channel, as must be the case in a dual model. Finally, it is impossible to calculate a simple dual amplitude using the Pomeron trajectory as the amplitude would be infinite for all values of the kinematic variables.

The Pomeron contribution is included by using a composite model in which a nondual Pomeron amplitude is added to a totally dual Veneziano amplitude. We discuss below these partial amplitudes and their method of combination.

A. The Pomeron Term

We treat the Pomeron contributions to this general reaction by considering diffraction-dissociation diagrams of the type shown in Fig. 1(a).[8] The exchanged trajectory is considered to be the Pomeron trajectory, and the upper vertex function is obtained from nucleon-nucleon elastic scattering data. While other trajectories could also be exchanged in this diagram, they are not since all non-Pomeron effects are included in the dual part of the composite amplitude. The lower vertex and accompanying lines of Fig. 1(a) are parameterized by the standard four-point Veneziano function in an effort to incorporate as much duality into the total scattering amplitude as possible. It would be possible to use other methods of parameterization of the lower vertex function, such as multi-Regge or resonance production models, but all such models must deal with the problems of double-counting and inclusion of proper diagrams which are avoided in the B_4 formulation.

While the Veneziano model only applies to reactions in which there are four real external particles, it may be extended to our case provided the Pomeron is considered to be a simple, spinless particle with a four-momentum Q which reacts with the other three legs of the lower vertex in the manner of a physical particle. This we are free to do since the form of the B_4 does not depend upon the masses of the external legs, but rather only upon the trajectories in the three invariant channels, which are determined by three external legs. It is only as an internal trajectory itself that care must be taken with the Pomeron in a dual amplitude.

We label a set of invariants as:

$$s = (N_i + \bar{N}_i)^2 \qquad s_1 = (\pi + N)^2$$

$$t = (\bar{N}_i - \bar{N})^2 \qquad t_1 = (N_i - N)^2$$

$$u_1 = (N_i - \pi)^2 \tag{1}$$

with the four-momenta as labeled in Fig. 1(a), and in terms of these, the Pomeron aplitude has the form:

$$M_{Pom} = \text{const. } e^{bt/2}(s/s_0)^{\alpha_{Pom}} V \tag{2}$$

where $e^{bt/2}$ is a simple diffractive parameterization for the nucleon-nucleon-Pomeron vertex, $(s/s_0)^{\alpha_{Pom}}$ is a Regge propagator for the Pomeron trajectory with $s_0 = 1\ \text{GeV}^2$ and $\alpha_{Pom} = 1$, and V is an amplitude for the lower Pomeron-nucleon-nucleon-pion vertex.

In general, the form of the lower vertex amplitude will be given by[8]

$$V = \bar{u}(N)\gamma_5[A(s_1, t_1, u_1) + \tfrac{1}{2}A'(s_1, t_1, u_1)\gamma_\mu(\pi^\mu + Q^\mu)]\,u(N_i) \tag{3}$$

where $\bar{u}$ and u are Dirac spinors for the initial and final nucleons and the term in brackets is the CGLN pion-nucleon decomposition.[9] A and A' are two invariant amplitudes as required by the two conserved values of total isospin for the pion-nucleon system and are assumed given by the Veneziano formula

$$A(s_1,t_1,u_1) = B[1-\alpha(s_1),1-\alpha(t_1)] + B[1-\alpha(s_1),1-\alpha(u_1)]$$
$$+ B[1-\alpha(t_1),1-\alpha(u_1)]$$

where

$$B(a,b) = \frac{\Gamma(a)\Gamma(b)}{\Gamma(a+b)}$$

is the Euler beta function. A similar expansion holds for the amplitude $A'(s_1,t_1,u_1)$.

In our reactions the Regge trajectories which couple to adjacent pairs of nucleon lines in the B_4 amplitudes are the π, ω, and A_1 trajectories.[10] It has been shown that the A_1 trajectory does not couple strongly to the N_i-N vertex[11] so we will not consider the contributions of the A_1 trajectory in our B_4 amplitude as a first approximation. Also, since the main contribution to the $A'(s_1,t_1,u_1)$ amplitude is from the A_1 trajectory, we drop the A' amplitude.[12]

Squaring and taking the spin sum of the amplitude in Eq. (3) (with $A' = 0$) gives

$$|V|^2 = (-t_1/s_0)|A(s_1,t_1,u_1)|^2$$

and hence the entire Pomeron term of Fig. 1(a) becomes

$$|M_{Pom}|^2 = \text{const. } e^{bt}(s/s_0)^{2\alpha_{Pom}(-t_1/s_0)}$$
$$\times |B[1-\alpha(s_1),1-\alpha(t_1)] + B[1-\alpha(s_1),1-\alpha(u_1)]$$
$$+ B[1-\alpha(t_1),1-\alpha(u_1)]|^2. \qquad (4)$$

B. The Dual Terms

The non-Pomeron terms of the composite scattering amplitude are treated with the generalization of the four-point Veneziano model to the case of a three-body final state. The generalization of the B_4 amplitude has been performed by Bardakci and Ruegg and is given by[5]

$$B_5[1-\alpha(x_1), 1-\alpha(x_2), 1-\alpha(x_3), 1-\alpha(x_4), 1-\alpha(x_5)]$$
$$= \int_0^1\int_0^1 \frac{du_i du_j}{1-u_i u_j} u_1^{-\alpha(x_1)} u_2^{-\alpha(x_2)} u_3^{-\alpha(x_3)} u_4^{-\alpha(x_4)} u_5^{-\alpha(x_5)} \qquad (5)$$

subject to the conditions

$$u_i = 1 - u_{i-1}u_{i+1} \; ; \quad i = 1 \ldots 5 \, .$$

In the above i and j may be any two nonconsecutive integers from one to five and x_1 through x_5 are the five invariants required by a three-body process. If we take all five of the external particles to be incoming as shown in Fig. 1(b), then a good set of invariants is:

$$x_1 = (P_1 + P_2)^2 \, , \qquad x_4 = (P_4 + P_5)^2 \, ,$$
$$x_2 = (P_2 + P_3)^2 \, , \qquad x_5 = (P_5 + P_1)^2 \, .$$
$$x_3 = (P_3 + P_4)^2 \, ,$$

The trajectories $\alpha(x_1)$ to $\alpha(x_5)$ are Regge trajectories and are taken to couple to adjacent pairs of external particles, as shown in Fig. 1(b). As in the four-point Veneziano model, however, there are several restraints

which must be placed on the trajectories. One of the steps in the development of the concept of duality from the finite-energy sum rules (FESR) requires that all of the resonances used in the FESR have zero-width and thus that the associated Regge trajectories be real.[13] Since the Veneziano amplitude incorporates the tenets of duality, it should also contain only real Regge trajectories if it is to preserve its developmental relationships. Similar restrictions require that the trajectories be linear and of uniform slope. It has been conjectured, however, that duality may constitute a basic principle in itself and need not depend upon these requirements,[13] and thus the Veneziano amplitude need not be bound to the use of unphysical trajectories. The Veneziano amplitude, calculated with complex trajectories of nearly the same slope, still embodies the property of correct Regge behavior and so physically realistic Regge trajectories are used in this model as a phenomenological necessity.

The B_5 amplitude as given in Eq. (5) contains all of the desired properties of a physical amplitude except crossing. In order to exhibit the proper crossing relations, the total five-point function must be a sum of all possible permutations of the external legs. Finally, the total amplitude must be multiplied by some kinematical factor (K) in an attempt to account for the spin of the external particles. The general dual amplitude is then given by

$$M_D = \text{const.}\,(K) \sum_{\text{Perm}} B_5(a,b,c,d,e) \ . \tag{6}$$

The kinematic factor K will be discussed in the following sections.

III. APPLICATION TO $\bar{p}p \to \bar{p}p\pi^o$

A. The Pomeron Terms

For the reaction $\bar{p}p \to \bar{p}p\pi^o$, there are two distinct Pomeron diagrams which must be considered. These are shown in Figs. 2(a) and 2(b). Before the Pomeron amplitude for this reaction can be written, three quantities must be specified: (a) the proper Regge trajectories to use in the B_4 amplitude at the lower vertices of Figs. 2(a) and 2(b); (b) the diffractive parameter to use in the upper vertex; and (c) the relative weight of the two diagrams in Figs. 2(a) and 2(b). These questions are considered in order below; for brevity only one of the diagrams is discussed.

In the Pomeron-p_i-p-π^o sub-reaction at the lower vertex of Fig. 2(a), there are several Regge trajectories which can be exchanged. The main trajectories which couple to two adjacent protons are the π, A_1, and ωA_2 where we assume the usual ωA_2 exchange degeneracy. For adjacent proton-pion lines any one of the N^* trajectories or the exchange degenerate (EXD) $\Delta_\delta - N_\beta$ trajectory may be used. All of these trajectories are possible in this reaction and the most rigorous procedure to follow is to include all of them in the scattering amplitude. Each diagram of Fig. 2 could be duplicated enough times so that each possible combination of trajectories would be represented, and then all such Veneziano terms summed. This method is rejected as impractical from a calculational viewpoint. Also, as it would require a separate parameter to specify

the relative amount of each diagram used in the amplitude, introducing a large number of free parameters. The path followed instead is to determine which of the above trajectories couples the most strongly to each vertex and then use only those trajectories; the resulting amplitude should then approximate the physical scattering process.

For two adjacent protons the trajectories considered are the π, A_1, and ωA_2, the ρ trajectory being excluded by G parity. As was mentioned in the previous section, the A_1 coupling is experimentally seen to be weaker than that of the π trajectory[11] and so it is neglected. The ωA_2 coupling is stronger than π coupling to pp vertices in other reactions[14] and thus, through factorization, we take the ωA_2 trajectory to dominate in our reaction.

Adjacent pion-proton pairs are treated by considering either the N^* trajectories or the $\Delta_\delta - N_\beta$ trajectory. Here there is no strong experimental evidence to suggest that any one of these trajectories will strongly dominate and so the choice is based on the experimentally observed final states of this reaction. There is strong delta resonance production in the data, while other nucleon resonances are not observed at our energy. Since the only method of delta production in this model involves the use of the delta trajectory, it is chosen over the other possibilities.[15]

The values taken for the trajectories are:

$$\alpha_\omega(x) = \theta(x_{th}-x)[0.48 + 0.9x] + \theta(x-x_{th})[0.48 + 0.9x + 0.07i\,(x-0.18)] \quad (7a)$$

$$\alpha_\Delta(x) = \theta(x_{th}-x)[0.13+1/2+0.9x] + \theta(x-x_{th})[0.13 + 0.9x + 0.14i\,(x-1)]. \quad (7b)$$

Here $\theta(z)$ is the step function in z, x represents any of the possible kinematic variables, and x_{th} is the threshold value for that channel. These values are the ones used by Chan, et al.,[14] and are obtained in a straightforward manner from the Particle Data Group tables.[16] When using the delta trajectory in a calculation, we use the quantity $[1 + 1/2 - \alpha_\Delta(x)]$ as an argument of the B_5 instead of the usual $[1 - \alpha_\Delta(x)]$ in order to produce resonances at the proper half-odd integer spin locations. This spin factor, however, yields the wrong intercept for the asymptotically exchanged delta trajectory, and in order to correct this problem, the trajectory below threshold is also shifted by a factor of 1/2.[14] Imaginary terms have been inserted into the trajectories above threshold to make them correspond to the physical world of finite-width resonances.

The diffractive parameter b in Eq. (2) for the Pomeron-$\bar{p}_i$-$\bar{p}$ upper vertex in Fig. 2(a) is obtained from the nucleon-nucleon elastic scattering data.[17] Parameterizing the elastic scattering process pp → pp as a simple exponential

$$\frac{d\sigma_{el}}{dt} = \text{const.} \times e^{2at} \tag{8}$$

yields a diffractive parameter of $2a \simeq 12$ $(\text{GeV/c})^{-2}$ for beam energies around 5 GeV.[18] Comparing this with Eq. (2) gives a value of $b \simeq 6$ $(\text{GeV/c})^{-2}$ to use in the Pomeron terms. A more appropriate way to obtain the value of b, however, is to compare the elastic scattering

data with Eq. (9) below. For $\bar{p}p \to \bar{p}p\pi^o$ the Pomeron contribution is

$$\left(\frac{d\sigma}{dt}\right)_{\text{Pomeron contribution}} = \text{const.} \times \int(\text{three-body phase space}) \times |M_{Pom}|^2 \qquad (9)$$

where $|M_{Pom}|^2$ is given by Eq. (4), and the integral is over all the kinematic variables excluding t. Since the only t-dependence in $|M_{Pom}|^2$ is in the exponential, the total t-dependence inside the integral of Eq. (9) is phase space times this exponential. The integral then gives

$$\left(\frac{d\sigma}{dt}\right)_{\text{Pomeron cont.}} = \text{const.} \times \left(\frac{d\sigma}{dt}\right)_{\text{phase space}} \times e^{bt} \; . \qquad (10)$$

The t-dependence of the phase space factor is simply the integral of Eq. (9) with $|M_{Pom}|^2 = 1$. The two Pomeron-p_i-p vertices in Eq. (8) must be compared with the one Pomeron-p_i-p vertex in Eq. (10) in order to get the correct value for the parameter b. Over much of the t range, the phase space factor does not change rapidly and frequently it is not necessary to consider it in making such a comparison. Calling phase space approximately a constant we would obtain $b \simeq 6$ $(\text{GeV/c})^{-2}$ as discussed above. However, because we are at a low momentum (2.9 GeV/c), and because most of the events we observe will occur at small values of -t, where phase space for t rises rapidly from zero, phase space cannot be considered a constant and must be included in the calculations. A numerical examination of the phase space factor yields the following relation

$$\left(\frac{d\sigma}{dt}\right)_{\text{phase space}} \simeq \text{const. } e^{-12t}, \quad 0 < -t \lesssim 0.3 \text{ GeV}^2 . \tag{11}$$

Using Eq. (11) in Eq. (10) and comparing with the data yields the value of $b \simeq 18$ $(\text{GeV}/c)^{-2}$ in order to get the correct slope at small values of $-t$.[19] This large value for b will, of course, produce a decreasing exponential with a slope of approximately 18 $(\text{GeV}/c)^{-2}$ for large values of $-t$, but that will occur far beyond the point at which the data has ceased to be a diffractive peak.

The last point considered in this section is the relative mixing of the two diagrams shown in Figs. 2(a) and 2(b). Since these two diagrams are simple charge conjugates, symmetry of the model under charge conjugation requires that the two diagrams be added equally and that they be in phase. The total squared amplitude for the Pomeron diagrams is then given by

$$\begin{aligned}
|M_{\text{Pom}}|^2 = \text{const.} \Big| & e^{18t/2}(s/s_0)^{\sqrt{-t_1/s_0}} \\
& \times \{B[\tfrac{3}{2}-\alpha_\Delta(s_1), 1-\alpha_\omega(u_1)] + B[1-\alpha_\omega(t_1), 1-\alpha_\omega(u_1)] \\
& + B[\tfrac{3}{2}-\alpha_\Delta(s_1), 1-\alpha_\omega(t_1)]\} \\
& + e^{18t'/2}(s'/s_0)^{\sqrt{-t_1'/s_0}} \\
& \times \{B[\tfrac{3}{2}-\alpha_\Delta(s_1'), 1-\alpha_\omega(u_1')] + B[1-\alpha_\omega(t_1'), 1-\alpha_\omega(u_1')] \\
& + B[\tfrac{3}{2}-\alpha_\Delta(s_1'), 1-\alpha_\omega(t_1')]\}\Big|^2
\end{aligned} \tag{12}$$

where the primed variables are the counterparts for Fig. 2(b) of the unprimed variables of Fig. 2(a).

B. The Dual Terms

In the general case of a three-body final state, there are twelve unique diagrams which must be considered in a dual model corresponding to all possible, noncyclic permutations of the legs of a five-point diagram. For the reaction $\bar{p}p \to \bar{p}p\pi^o$, however, only four possible diagrams are considered as the other diagrams require the exchange of exotic trajectories and so are discarded. The diagrams which must be considered are shown in Fig. 2(c). The Regge trajectories shown as coupling to adjacent external legs are the same as those discussed in previous sections and have been chosen for the reasons given there. The trajectories shown in Fig. 2(c) are expected to dominate, and these four diagrams to be a good approximation to the physical scattering process.

The kinematical factor K which multiplies each B_5 term in Eq. (6) is treated in two different manners. One choice is to make the observation that each internal trajectory begins with a p-wave resonance and thus takes an invariant of the form[20]

$$K = \epsilon_{\mu\nu\rho\sigma} P_1^{\mu} P_2^{\nu} P_3^{\rho} P_4^{\sigma} \tag{13}$$

to multiply each B_5 amplitude, where P_1 through P_4 are any four of the five four-momenta associated with the reaction, and $\epsilon_{\mu\nu\rho\sigma}$ is the fourth-ranked Levi-Civita symbol. We use the Einstein summation convention on repeated indices. A factor such as the one above is needed in the theory of the Veneziano five-point function so that the asymptotic limits are polynomials of the correct degree in the kinematic variables as required

by Regge theory.[21] The factor in Eq. (13) is the simplest Lorentz invariant which can be constructed out of four four-momenta and so is not an unexpected choice. The second method used is to simply replace the spin factor with unity. This is done in order to examine the bare dual model apart from the effects of the spin factor. This second method is worth pursuing as, while some factor similar to that given in Eq. (13) is necessary for the asymptotic limits of this model, it is not obvious that Eq. (13) is the proper one to use for this reaction nor is it obvious what the form of such a factor should be at low experimental energies.

The final consideration given to the dual amplitude is the relative mixing of the four diagrams shown in Fig. 2(c). The simplest observation is that diagrams $B_5(1)$ and $B_5(1')$ are charge conjugates and again invariance under charge conjugation will require that these two diagrams be added equally and that they be in phase. The remaining two diagrams can both be eliminated since they can both be obtained from diagrams $B_5(1)$ and $B_5(1')$ under an interchange of the lines of a πp or $\pi\bar{p}$ pair of external particles. That is, interchanging the lines of the outgoing $\pi^o\bar{p}$ pair in diagram $B_5(1)$ will produce diagram $B_5(2)$, and so on. If the $\Delta_\delta - N_\beta$ trajectory is assumed to be totally exchange degenerate, then both diagrams $B_5(1)$ and $B_5(2)$ may not be included since to do so would make the trajectory totally nonexchange degenerate (NED) in this model. Thus we do not keep diagram $B_5(2)$; similarly, diagram $B_5(3)$ is discarded. Thus the final squared amplitude is

$$|M_A|^2 = D|M_{Pom}|^2 + |\epsilon_{\mu\nu\rho\sigma} P_1^\mu P_2^\nu P_3^\rho P_4^\sigma$$

$$\times B_5[\tfrac{3}{2} - \alpha_\Delta(t_{\bar{p}_i\pi^o}), \tfrac{3}{2} - \alpha_\Delta(s_{\pi^o\bar{p}}), 1 - \alpha_\omega(s_{\bar{p}p}), 1 - \alpha_\omega(t_{pp_i}),$$

$$1 - \alpha_\omega(s_{p_i\bar{p}_i})] + \epsilon_{\mu\nu\rho\sigma} P_1^\mu P_2^\nu P_3^\rho P_4^\sigma$$

$$\times B_5[1 - \alpha_\omega(t_{\bar{p}_i\bar{p}}), 1 - \alpha_\omega(s_{\bar{p}p}), \tfrac{3}{2} - \alpha_\Delta(s_{p\pi^o}),$$

$$\tfrac{3}{2} - \alpha_\Delta(t_{\pi^o p_i}), 1 - \alpha_\omega(s_{\bar{p}_i p_i})]|^2 \qquad (14)$$

where $|M_{Pom}|^2$ is given by Eq. (12) with the value b = 18 $(GeV/c)^{-2}$, and the variables in the B_5 terms are the invariants constructed from the four-momenta of the particles indicated. D is an unknown parameter. This model we call the "best theoretical" model (and also Model A), and apart from the overall normalization contains only the one free parameter D which determines the relative amount of Pomeron to dual contribution.

In addition to Model A given above, two other models are formed with which the data are examined to see the effect of relaxing some of the theoretical requirements. The first of the other models is labeled Model B and in it all four of the dual diagrams shown in Fig. 2(c) are present, and each of these diagrams is weighted by a parameter determined by fitting the data. Charge conjugation symmetry is still included in the model and thus diagrams $B_5(1)$ and $B_5(1')$ are left in a unit and in phase. This gives Model B:

$$|M_B|^2 = D|M_{Pom}|^2 + (\epsilon_{\mu\nu\rho\sigma}P_1^\mu P_2^\nu P_3^\rho P_4^\sigma)^2 \times \{D_1|B_5(1)+B_5(1')|^2$$

$$+ D_2|B_5(2)|^2 + D_3|B_5(3)|^2\} . \qquad (15)$$

In Eq. (15) we have labeled the dual terms by their labels as given in Fig. 2(c) for simplicity. Each B_5 term has a form similar to those in Eq. (14) and can be easily constructed by inspection. This model again uses Eq. (12) for $|M_{Pom}|^2$ and takes $b = 18\ (GeV/c)^{-2}$. There are then the four parameters D, D_1, D_2, and D_3 subject to the one constraint of overall normalization.

Finally, Model C is identical to Model B except that the kinematic factor $\epsilon_{\mu\nu\rho\sigma}P_1^\mu P_2^\nu P_3^\rho P_4^\sigma$ has been replaced with unity. Model C is given in Eq. (16). The results obtained from each of these three models will be discussed in the following sections.

$$|M_C|^2 = D|M_{Pom}|^2 + \{D_1|B_5(1)+B_5(1')|^2 + D_2|B_5(2)|^2 + D_3|B_5(3)|^2\} . \qquad (16)$$

The calculations were performed on the IBM 360/65, and on an EMR 6050 using standard Monte Carlo methods of numerical integraion and making use of the series decomposition of the B_5 developed by Hopkinson and Plahte.[22] Enough events were generated to assure smooth functions for the integrals. All of the theoretical curves shown below have been smoothed by an interpolative computer plotting program.[23]

IV. COMPARISON WITH THE DATA

In this section we examine our models for the reaction $\bar{p}p \rightarrow \bar{p}p\pi^o$ with the data at a beam momentum of 2.88 GeV/c.[24] We first give a brief description of the method used to decide upon the quality of a particular fit, and then give some examples of the uncombined squared amplitudes for the diagrams shown in Fig. 2. Next the fits obtained for each of the Models, A, B, and C are described and finally we give a comparison of the three different models.

A. Kinematics and Diagrams

Before we can compare the models with the data, we must first discuss the method used to determine the quality of a given fit. One possible approach is to form histograms of particular interest, such as invariant masses in which one expects to find interesting structure, and calculate the chi-square from the fit to each of these histograms. The set of parameters which gave the lowest chi-squares would then be the best fit to the data. A problem in this method, however, is that it is not obvious which set of histograms should be examined, and a good fit in terms of one set may not appear to be a good fit when viewed under a different set. If, for example, one had a model which accurately reproduced resonances in invariant mass plots, but could not produce good t distributions, it would seem to fit data better if one looked at only a set of invariant masses than it would if one looked at all t plots. Another method with which data might be examined is to use a

"usual" set of invariant histograms: the incoming s-channel, two outgoing s-channels and two peripheral t-channels such as are shown in the diagram in Fig. 3. This is no better than the previously discussed method as, while it does give a specific set of histograms, there is no reason that this set could not also be unrepresentative of a given model or fit.[25]

We use the following method of comparison: we form the ten simple invariants which can be made out of the five-four-momenta taken two at a time, given in Eq. (17). (See Fig. 2(c).)

$$
\begin{aligned}
s &= (p_i + \bar{p}_i)^2 & t_{\bar{p}_i \bar{p}} &= (\bar{p}_i - \bar{p})^2 & t_{\bar{p}_i p} &= (\bar{p}_i - p)^2 \\
s_{\bar{p}\pi} &= (\bar{p} + \pi)^2 & t_{p_i p} &= (p_i - p)^2 & t_{p_i \bar{p}} &= (p_i - \bar{p})^2 \\
s_{p\pi} &= (p + \pi)^2 & t_{\bar{p}_i \pi} &= (\bar{p}_i - \pi)^2 & & \\
s_{\bar{p}p} &= (\bar{p} + p)^2 & t_{p_i \pi} &= (p_i - \pi)^2 & & \qquad (17)
\end{aligned}
$$

where the four-momenta are defined by

p_i = incoming proton four-momentum,

$\bar{p}_i$ = incoming antiproton four-momentum,

$\bar{p}$ = outgoing antiproton four-momentum,

p = outgoing proton four-momentum,

π = outgoing pion four-momentum .

Histograms made from these ten invariants then correspond to all of the simple projections of a five-dimensional Dalitz plot onto a one

dimensional space. The best possible parameterization is then defined as the one which agrees the closest with data for all of the ten histograms. To do this, the chi-square of a fit for each histogram is calculated and the ten chi-squares are added together. The fit with the lowest chi-square sum then represents the best agreement with the data. As a practical point, the contribution to this sum from the histogram of the invariant s will always be the same at a given energy and so we ignore this invariant. Finally, dividing the total sum by the number of histograms, nine, gives an "average" chi-square for the overall fit.

The fitting procedure in general consists of determining the relative amounts of the Pomeron diagrams to be added to the dual diagrams, and also the relative amounts of each of the dual diagrams to include in the total differential cross section in order to best fit the data. In Fig. 4 are shown five representative histograms considered for each of the Pomeron and dual diagrams of Fig. 2^{26} together with the data.

In Fig. 4 only five of the nine histograms are shown as it would be uninstructive to show the remaining four. The $M_{\bar{p}\pi}$ histogram appears to be virtually identical to that of $M_{p\pi}$ for instance, although the chi-squares obtained from the two distributions are not equal. In Fig. 4 we have set up labels for each of the histograms which shall be used throughout the paper. For example, the invariant mass $M_{p\pi}$ will always be referred to as histogram number 1.

One important observation which can be seen in the theoretical curves of Fig. 4 is the very pronounced peripherality exhibited in the

Pomeron diagrams. The lack of such sharply peaked structures in the dual diagrams is a clear indication that the Pomeron diagrams will indeed contribute strongly to the total cross sections and that the data could not be well fit using only a pure dual model. A second important observation is, except for the peripherality of the Pomeron diagrams, the similarity of the predictions of the Pomeron, $B_5(1)$ and $B_5(2)$ diagrams, while the prediction of $B_5(3)$ is markedly different. Because of the lack of structure in the $B_5(3)$ diagram, we label it a "background" diagram, and as we shall see later in this section, it will be an exceedingly important diagram as it is the only one which is able to fill in parts of the data which correspond neither to resonances nor to other strong structures such as sharp t distribution.[27]

B. Model A

The first model considered is the "best theoretical calculation," Model A, given in Eq. (14). In this model there are only the dual diagrams $B_5(1)$ and $B_5(1')$ and, apart from the overall normalization of the cross section to the data, only the one parameter D which determines the relative amount of Pomeron to dual contributions to the cross sections. The best fit to the data occurs for the value of the parameter $D = 9.79\times(10)^{-4}$ and this fit has an average chi-square of 139 for the nine histograms when they are each divided into fifty bins. In Fig. 5(a) five of the nine histograms generated from this model are shown along with the $\bar{p}p \to \bar{p}p\pi^o$ data (2.88 GeV/c).

The method used to obtain this fit was the following: first, the cross section for Model A for a given value of the parameter D was calculated. The calculation was then normalized in order to agree with the data and the chi-squares for each histogram were computed, after which the chi-squares were added together and divided by the number of histograms to get an average chi-square per histogram for that value of D. Finally, D was varied in steps over a large range of possible values, and the set of average chi-squares that were generated was examined. We found the chi-square to be a relatively smooth function of the value of the parameter. The behavior of this function in the region of the obvious minimum chi-square was examined in steps in the value of D approximately two orders of magnitude smaller than the first steps. This showed the function to be in fact very smooth, and from the second set of chi-squares we found the minimum and its corresponding value of D which we have quoted.

Rewriting Eq. (14) in terms of a Pomeron and a dual term as

$$|M_A|^2 = D|M_{Pom}|^2 + |M_{Dual}|^2 , \tag{18}$$

where $|M_{Dual}|^2$ is defined by Eq. (14), allows one to discuss the free parameter D in this model in terms of a more meaningful quantity. Normalizing Eq. (18) to the data and defining the quantity R as the ratio of the Pomeron to the dual terms in the normalized square amplitude gives

$$R \equiv \frac{D\int |M_{Pom}|^2 d(\text{phase space})}{\int |M_{Dual}|^2 d(\text{phase space})} \quad . \tag{19}$$

Thus, R measures the total contribution of the Pomeron terms to the cross section relative to the dual terms without including the inherent differences in size of the unnormalized $|M_{Pom}|^2$ and $|M_{Dual}|^2$ terms. The best fit of Model A has a value R = 1.15.

In Fig. 6 we present a plot of the chi-square values found for Model A as a function of both D and R. Values of the parameter to the left of zero are physically impossible, and values beyond the right edge of the graph rise uniformly to a chi-square of slightly above 225, which represents an essentially pure Pomeron model.

The curves for Model A shown in Fig. 5(a) are seen to agree with the overall structure of the data, but they do exhibit some features not in keeping with the experimental facts. Perhaps the most serious discrepancies occur in the two histograms in which the $\Delta(1236)$ resonance is seen, the outgoing $\pi^o p$ and the outgoing $\pi^o \bar{p}$ systems. The theory in both of these graphs produces the delta resonance more strongly than is seen in the data, and also with half-widths which are too wide. In addition, the high mass tails in both of these distributions drop off too quickly. Another problem occurs in histogram number 2 involving the two outgoing nucleons. The theory here shows a large discrepancy in the low mass tail and has an overabundance of events in the higher mass regions. The theory in all of the histograms, in fact, is unable to accurately reproduce either high or low energy tails. In general, the major problem

with this model is that while it can produce structure, e.g., resonances, well it cannot adequately fit the background on which the structure exists. This is not an unexpected result, however, since Model A does not contain diagram $B_5(3)$, the "background" diagram. As we shall see, the inclusion of diagram $B_5(3)$ in later models will alleviate this problem to a large extent.

One further problem with this model is that in the peripheral t histograms (number 3 in Fig. 5(a)) the forward peaks are not as sharp as the data would indicate. This suggests that we should have taken a slightly larger diffractive parameter b for the Pomeron amplitude in Eq. (4). We estimate that a value of $b \simeq 20$ $(\text{GeV/c})^{-2}$ would slightly better reproduce the data, indicating that either the phase space factor attenuates the slope of the exponential more than had been expected or that there is some other t-dependence in the Pomeron amplitude which needs to be considered.

C. Model B

The second model considered contains all four of the dual diagrams shown in Fig. 2(c), and also includes the kinematic spin factor. This is Model B and is given by Eq. (15). Model B includes, apart from the overall normalization, a total of three parameters which determine the relative amounts of the contributions to the cross section of the different diagrams; these parameters are allowed to vary in order to give the lowest value of the average chi-square, as was done with Model A. The best fit to the data occurs for the following values of the

parameters of Eq. (15): $D_1 = 1/4$, $D_2 = 1/4$, and $D_3 = 1$, along with the factor $D = 1.32 \times (10)^{-3}$ multiplying $|M_{Pom}|^2$. This parameterization produces an average chi-square of 90.3 for the nine histograms. Defining R for this model in a manner analogous to that used for Model A, the best parameterization of Model B has a value $R = 1.48$.

In Fig. 5(b) are the histograms obtained from this parameterization of Model B along with the data. In Fig. 7(a) are shown the decay angular correlations of the $\Delta(1236)$ in terms of the Jackson angle θ[28] and the Treiman-Yang angle ϕ[29] which are calculated in the rest frame of the outgoing πp system. These angular contributions were not considered in the determination of the parameters for this model, but are rather a prediction of the model.

In finding the optimum parameterization of Model B we have used essentially the same procedure described in connection with Model A generalized to the case of three free parameters. We varied in a systematic manner a total of four quantities, the three parameters, D_1, D_2, and D_3, and the factor D which multiplied $|M_{Pom}|^2$. Then the average chi-squares obtained from this search were examined, the regions around the minimums were re-examined, and the parameterization shown above was chosen as the best fit. In Model B instead of having one well-defined minimum from which the parameter could not deviate greatly without an accompaning large increase in the average chi-square, as was the case for Model A, there is a volume in the parameter space which produces chi-squares slightly larger than the one quoted for the minimum. Some representative sets of parameters which lead to average chi-squares on

the order of the minimum are shown in Table 1.

It is clear from Table 1 that Model B is somewhat insensitive to the particular parameters one chooses, although some general trends can be discerned. While there are several sets of parameters all of which are nearly comparable, they all exist within a fairly small volume of the parameter space. The other parameter sets looked at show that travel in any direction out of the general volume represented in Table 1 indeed quickly increases the value of the average chi-square, i.e., radically different parameterizations produce average chi-squares significantly larger. Physically, the requirements for a small chi-square are that the Pomeron diagrams be added about equally to the dual $B_5(3)$ diagram with a slight contribution from the other dual diagrams. The total cross sections obtained from each of the dual diagrams are, when unnormalized, approximately equals in magnitude, so that a parameterization of $D_2 = 1/4$ and $D_3 = 1$ yields a ratio of about four to one for the effective contributions of diagrams $B_5(3)$ and $B_5(2)$. Using only the Pomeron and $B_5(3)$ diagrams does not give a low chi-square for this model and also using the diagrams Pomeron, $B_5(1)$ and $B_5(3)$, is preferable to using Pomeron, $B_5(2)$ and $B_5(3)$. Excluding either the Pomeron or the $B_5(3)$ diagrams makes it impossible to obtain an average chi-square lower than the 139 produced by Model A.

While Model B contains many of the same problems as found in Model A, it fits the data considerably better. Again the peripheral t distributions in histogram 3 of Fig. 5(b) do not peak as early as the data, however, now the tails of these diagrams correspond to the data

better. The backward t distribution of histogram 5, taken between the incoming p and the outgoing $\bar{p}$, shows an enhanced should above the region $-\sqrt{-t} = -1.4$ GeV, which is a problem with this fit. Through the use of a different parameterization for Model B, these shoulders can be eliminated but not without the expense of worsening the remaining seven histograms. The theoretical curve in histogram 3, containing the two outgoing nucleons, is seen to be significantly improved over Model A in that it can fit the background tail quite well. In general, the most striking difference between Models A and B is the ability of Model B to fill in the regions of the histograms which do not correspond to the areas in which strong structures such as resonances, are present. This is due almost entirely to the inclusion of the dual "background" diagram $B_5(3)$.

Finally, the curve in histogram 1 again shows a difficulty in its ability to perfectly fit the $\Delta(1236)$ resonance. As in Model A, the Δ's produced through this model are both stronger and broader than the data. They are, however, considerably closer to the data than those of Model A and so contribute considerably less to the average chi-square for the fit. There also is seen to be an enhancement or perhaps a second resonance in the region of 1580 MeV which is produced by the J = 5/2 pole of the totally exchange degenerate Δ_δ-N_β trajectory. Since this resonance is not very pronounced in the data, we should perhaps consider a slightly broken EXD for these two trajectories, although the breaking would have to be fairly small. Taking these trajectories as totally NED,

however, would still produce an enhancement at this mass due to the non-canceled first daughter of the Δ_δ trajectory.

The last comparison we make for this model is in the angular distribution of Fig. 7(a). The Jackson angle is seen to agree very well with the data while the Treiman-Yang angle shows serious discrepancies. While this causes definite problems with our fits, it is a common problem with dual models of this type and represents an area of needed improvement.

D. Model C

The final examination of this reaction uses Model C, given in Eq. (16), which is identical to Model B just discussed except that the kinematic spin factor K defined for Model B in Eq. (13) has been replaced with unity. We follow the same procedure used for Model B in order to determine the best fit for this model, and obtain an optimum average chi-square for the following set of parameters: $D_1 = 0$, $D_2 = 0$, and $D_3 = 1$ along with the factor $D = 6.01 \times (10)^{-5}$ multiplying the Pomeron terms in Eq. (16). This set of parameters yields an average chi-square of 65.8 and has a ratio of Pomeron to dual contributions of $R = 0.4$. In Fig. 5(c) are shown the histograms for this fit and in Fig. 7(b) the Jackson and Treiman-Yang angles for the delta decay as described in the discussion of Model B; again these latter distributions are predictions.

Unlike Model B in which the chi-square function was not too sensitive to the particular set of parameters within a certain volume of the

parameter space, Model C is quite restrictive in the parameters which produce a small average chi-square. Slight changes in the ratio R do not drastically effect the average chi-square, but almost any attempt to change the parameters D_1 or D_2 from zero causes this average value to quickly rise to around 90. A small region in the parameter space inside which the chi-square function is relatively constant does exist, however. This is a region approximately bound by the following values of the parameters: $0 \leq D_1 \leq 0.13$, $0 \leq D_2 \leq 0.13$, and $0.2 \leq R \leq 0.4$, with D_3 remaining at approximately unity. Within this region, the average chi-square ranges from a low of 65.8 for the optimum parameterization to a high of 85 for each parameter at its upper bound and increases fairly uniformly as the sum $D_1 + D_2$ increases.

It is clear that in Model C nearly all of the cross sections is due to the dual diagram $B_5(3)$ with essentially no contribution from the other dual diagrams, and further that the Pomeron diagrams account for only a small fraction of the total cross section. This parameterization is very different in content from those of the previous models; it can be understood from the following considerations. The theoretical curves produced by the Pomeron diagrams consist almost entirely of very sharp structure sitting on virtually no background, while those coming from the dual diagrams $B_5(1)$ and $B_5(2)$ do not have such well-defined and sharp structures and have quite a bit of background. In particular, the $\Delta(1236)$ produced in the dual diagrams is considerably broader and more diffuse than the one obtained from the Pomeron diagrams. The dual diagram $B_5(3)$ contains almost no structure and is essentially

pure background. Because the $\Delta(1236)$ is produced rather weakly in the data, it is possible for the background dual diagram and the Pomeron diagrams alone to fit the histograms containing the delta, number 1 of Fig. 5(c); since the Pomeron diagrams contain the strong structure found in the remaining histograms, this combination of diagrams can also reproduce the other histograms. If the delta were a stronger signal in the data, it would be necessary to include the other dual diagrams as the Pomeron could not fit a strong delta resonance, its delta being both too sharp and too narrow.

The small Pomeron to dual ratio, measured by the quantity R, is possible since the only dual diagram used in this parameterization is the background diagram, the Pomeron does not have to compete with the other dual diagrams in order to correctly produce the peripheral t peak in histogram 3. That is, previously a large Pomeron term was required in order that ths slope of these two histograms be correct as it had to overcome the incorrect t-dependence in the diagrams $B_5(1)$ and $B_5(2)$ whereas now it does not.

It should be mentioned that the reason Model C is able to fit the data better than Model B is because of the exclusion of the kinematical factor K of Eq. (13) rather than simply the different parameter values. If the Model C parameters given above are used in Model B, the resultant average chi-square is approximately 350.

As was the case for Model B, Model C exhibits quite good agreement with the data. Indeed, there is little difference between the results for these two models except in the distributions containing the delta

resonances, histogram 1 of Fig. 5(c). Whereas in Models A and B the $\Delta(1236)$ resonances were produced much more strongly and with significantly broader half-widths than shown in the data, Model C contains only very slight delta production. Indeed, looking at the theory apart from the data, one would be inclined to discount Model C because of its near lack of the delta resonance. The main contribution to the lower average chi-square for this model relative to Model B is due to these two histograms, however, as these histograms have individual chi-squares for Model C which are approximately one-half of the chi-squares involved in Model B.

Aside from this peculiarity, Model C is very representative of the data. In the histograms mentioned above the enhancement in the region of 1580 MeV seen in Model B no longer occurs. The fit in the remainder of the histograms has also improved. The peripheral peaks of the t distributions in histograms 3 and 5 now occur at the same locations in both the theory and in the data, and their tails are in good agreement to the data. Finally, the shoulders which were present in histogram 5 of Model B are gone from this model.

The angular plots are impressive when compared with those of Model B. While the Jackson angle θ has not changed greatly, the Treiman-Yang angle is better in this model by almost a factor of three in the individual chi-square over that obtained from Model B. In summary, this model reproduces the data well.

E. Summary

Several conclusions can be drawn from the comparison of the three models with the data for the reaction $\bar{p}p \rightarrow \bar{p}p\pi^{o}$. The first conclusion is that the best theoretical calculation, Model A, is seen to do amazingly well considering the little freedom which it has to fit the data. It is quite interesting that such a simple model, containing only one free parameter, is able to reproduce the data as well as it does. Looking at Models B and C it is not surprising that they are better able to fit the data since they do have more free parameters, although still they do not have many. We would conclude from Model C that the kinematical spin factor K has a substantial effect upon the theory at our energy, and that it has a detrimental effect for the reaction $pp \rightarrow pp\pi^{o}$. Obviously, had the data shown a more pronounced $\Delta(1236)$ resonance, our best parameterization of Model C would not have agreed with the data as well as it did, but we believe it still would have done better than any parameterization of Model B could have done. This result would suggest that different forms for the spin factor be examined in order that one may be found which can both satisfy the asymptotic requirements and also agree with the data at experimental energies. Finally, it is necessary to include the effects of phase space into the determination of the Pomeron-p-p vertices, at least at the energy of this reaction.

V. APPLICATION TO $\bar{p}p \rightarrow \bar{p}n\pi^{+}$

In this section we follow the procedure discussed in the previous sections to examine the two remaining states of the one pion production

reactions: $\bar{p}p \rightarrow \bar{p}n\pi^+$ and $\bar{p}p \rightarrow p\bar{n}\pi^-$. Both of these final states are treated simultaneously since they are simple charge conjugates and hence should be the same. As this model makes no distinction between these two final states, only the final state $\bar{p}n\pi^+$ is considered and the combined data from these two final states are examined. In the remainder of this section we discuss first the Pomeron diagrams applicable to these reactions, and then the dual diagrams to be considered. The models to be examined are presented, and the results obtained from each are given. Finally, we discuss the ability of each of our models to fit these data.

A. Pomeron Term

There is only one possible Pomeron diagram which can contribute to this reaction since the charged pion must be produced at the neutron vertex. This diagram is shown in Fig. 8(a); it is identical to those which we used for the previous reaction, and is calculated in the same manner. We use the value of the Pomeron-$\bar{p}_i$-$\bar{p}$ diffractive scattering parameter at the upper vertex which was obtained before and couple the adjacent πp lines to the delta trajectory in the lower B_4 vertex. The adjacent πn lines are likewise coupled to the delta trajectory. The only difference which occurs in the calculation of this diagram from that of the previous reaction is in the trajectory which couples to adjacent pn lines. The ω trajectory cannot be used as was done for adjacent pp lines as it cannot account for the charge difference which is at this vertex. The pn external line pairs are coupled to the π trajectory. The A_1 trajectory is not used because of the arguments given in the previous

reaction. The value for the π trajectory is obtained from the Particle Data Group tables,[16] while the imaginary part of the trajectory above threshold is calculated from the formula[14]

$$\mathrm{Im}\alpha = \alpha' M_{res} \Gamma_{res} ,$$

where α' is the slope of the real part of the trajectory, M_{res} and Γ_{res}, are the mass and half-widths of resonances on the trajectory, respectively. The parameterization of the π trajectory is

$$\alpha_\pi(x) = \theta(x_{th}-x)[-0.02+0.9x] + \theta(x-x_{th})[-0.02+0.67x+0.07i\,(x-0.18)]$$

where as before θ is the step function, and x is used to represent the squared invariants of the reaction.

Following the procedure used in the previous reaction, the Pomeron term is

$$\begin{aligned} |M_{Pom}|^2 = \text{const.} \times & \left| e^{18t/2} (s/s_0)^{\sqrt{-t_1/s_0}} \right. \\ & \times \{B[\tfrac{3}{2}-\alpha_\Delta(s_1),-\alpha_\pi(t_1)] + B[\tfrac{3}{2}-\alpha_\Delta(s_1),\tfrac{3}{2}-\alpha_\Delta(u_1)] \\ & \left. + B[-\alpha_\pi(t_1),\tfrac{3}{2}-\alpha_\Delta(u_1)]\} \right|^2 \end{aligned} \qquad (20)$$

where the invariants are defined by Eq. (1), substituting the outgoing neutron for the outgoing proton.

B. Dual Terms

As was the case in the previous reaction, there are only four dual diagrams which need be considered for the reaction $\bar{p}p \to \bar{p}n\pi^+$ as the

other eight all involve the use of exotic trajectories; the four diagrams are shown in Fig. 8(b). We make the same choice for the Regge trajectories as before except that the π trajectory couples to adjacent proton-neutron legs for the reasons discussed in the Pomeron section of this reaction.

Unlike the case involving the neutral pion, very little can be said about the manner in which these four diagrams should be combined in order to form the complete dual amplitude, however, one determination is possible and this is used in constructing our dual terms. Diagrams $B_5(1)$ and $B_5(1')$ of Fig. 8(b) differ only in the interchange of the incoming $\bar{p}_i$-π^+ lines. These lines must couple to the double charged delta when both particles are taken as incoming. Since the Δ^{++} is known not to have a $5/2^-$ partner, it must be taken to be totally non-exchange degenerate (NED). In order to accomplish this, diagrams $B_5(1)$ and $B_5(1')$ must be combined equally and in phase as any other combination would produce an exchange degeneracy due to the structure of the B_5 amplitudes. We are not able to make any other statements regarding the relative mixing of these four diagrams and so take the remaining two mixing constants to be free parameters as was done in Models B and C of the previous reaction.

The one final decision which must be made before this model can be examined is on the inclusion of the kinematic spin factor which must be used in Eq. (6) to attempt to account for the asymptotic behavior of the amplitude. As the pion trajectory does not begin with a p-wave resonance, as do the trajectories used for the π^o final state,

the spin factor used in Models A and B given by Eq. (13) cannot be used here. Instead the present procedure is based upon the results of the previous section and uses a factor of unity in the model. Unity is chosen over some more complicated factor in order to examine the ability of the basic model to reproduce the data.

The dual amplitude is calculated in precisely the same manner as done previously. Combining the dual and the Pomeron terms gives the model for this reaction (Model D):

$$|M_D|^2 = D|M_{Pom}|^2+D_1|B_5(1)+B_5(1')|^2+D_2|B_5(2)|^2+D_3|B_5(3)|^2, \qquad (21)$$

where $|M_{Pom}|^2$ is given in Eq. (20), D, D_1, D_2, and D_3 are four parameters subject to one overall normalization constraint, and $B_5(1)$ represents the dual amplitude for diagram 1 in Fig. 8(b) and has the form of the dual amplitudes given in Eq. (14). The argument of the pion trajectory in the dual amplitudes is $[0-\alpha_\pi(x)]$ as was the case in the Pomeron amplitude for this reaction.

C. Comparison with the Data

The method by which we compare this model with the data and determine the degree of the fit is identical to that used for the $\bar{p}p\pi^o$ final state. In Fig. 9(a) is shown seven of the histograms for the diagram $B_5(1')$ of Fig. 8(b). These are the five shown for the π^o final state and an additional invariant mass and t distribution. Unlike the first reaction studied, the $\bar{p}n\pi^+$ final state is not symmetrical in that

some, but not all, of the ω trajectories have been replaced with π trajectories. Hence diagram $B_5(1')$ of Fig. 8(b), for example, will yield a different theoretical curve for the t-distribution taken between the incoming and outgoing antiprotons than it will for the one taken between the incoming proton and outgoing neutron. The two additional histograms shown are those which differ the most from their counterparts (i.e., $M_{\pi\bar{p}}$ and $M_{\pi n}$). The remaining two t-histograms are quite similar to the ones shown.

One immediate observation to make is that although diagram $B_5(1')$ is identical to the diagram $B_5(3)$ of the neutral pion final state, except for its trajectories, it no longer produces the very smooth behavior which we have labeled "background" that it did in the previous reaction. Indeed, none of the present diagrams contain such complete lack of structure. It is also interesting at this point to notice the very distinct differences which have occurred in some of the dual diagrams in going from the $\bar{p}p\pi^o$ to the $\bar{p}n\pi^+$ reaction, and which are caused by the simple replacement of the ω trajectory with the π trajectory; we return to this difference later in this section.

We now proceed to examine the model with the combined data for the reaction $\bar{p}p \rightarrow \bar{p}n\pi^+$ and $\bar{p}p \rightarrow p\bar{n}\pi^-$. The best fit for this model has the following parameterization: $D_1 = 0$, $D_2 = 3/4$, $D_3 = 1/4$, and $D = 3.7$. This has a value for the Pomeron to dual ratio of $R = 2.5$ and yields an average chi-square of 1420. The histograms for this model are shown in Fig. 9(b).

In the search for an optimum set of parameters for this reaction, we find that no set yields a good fit to our data. Further, the different choices of parameters do not greatly effect the average chi-square; changing the parameters varies the average chi-square over a range of approximately 35% of the minimum. The best fit is not unique as several other sets of parameters also give average chi-squares comparable to the one we list as the minimum, but these other sets lie within a relatively small region in the parameter space; this region was not examined in great detail as the quality of this fit does not merit much effort.

The primary reason for the failure of Model D to agree with the $\bar{p}n\pi^+$ data is connected with the use of the π trajectory in the B_5 dual amplitudes. Calculating cross sections using the π trajectory we do not obtain results which are similar in nature to those obtained using other trajectories. For example, when the ω trajectory is replaced with the π trajectory, any form of background-like behavior is totally eliminated from the histograms for the individual dual diagrams. In the $\bar{p}p \rightarrow \bar{p}p\pi^o$ reaction where the ω trajectory was used, histograms for diagram $B_5(3)$ were smooth and lacking in structure. In the present case using the π trajectory, however, even though there is an equivalent diagram, such a uniform lack of structure is unobtainable. The markedly different behavior of the dual diagrams for the two different final states is a function strictly of the use or nonuse of the π trajectory. Replacing the ω trajectory with any Regge trajectory other than the π would not have caused such radically different results.

Thus, in the B_5 formulation, the π trajectory is unique in that amplitudes generated using it are not similar to those generated using any other Regge trajectories.[30]

The inability of this model to fit the charged pion final state data is a direct result of the lack of background-like behavior in the dual diagrams; there is no possible way in which those parts of the data which do not correspond to strong structure can be fit. As we are able to fit only resonances and peripheral t distributions, and not the background on which they sit, we are unable to arrive at a good average chi-square with this model.

Because of the failure of Model D, we choose one final manner by which to examine these data. In order to appreciate the extent of the inability of this dual model to contain the pion trajectory, we consider the unphysical case in which the proton and neutron are taken to be identical particles and try to fit the data with one of the models used in the $\bar{p}p \to \bar{p}p\pi^o$ reaction. Specifically, we take Model C in its entirety and apply it to the data of the combined $\bar{p}n\pi^+$ and $p\bar{n}\pi^-$ final states. We use this model for simplicity as it will best show the effects of replacing the ω trajectory with the π trajectory without the additional complications of the spin factor. The two dual diagrams $B_5(1)$ and $B_5(1')$ are still combined equally as before, and the model as given in Eq. (16) of the previous section is used. Following the usual procedure we find the best fit the parameters $D_1 = 0$, $D_2 = 0$, $D_3 = 1$ and with the ratio of Pomeron to dual contribution $R = 0.2$. This has an average chi-square of 572. We show this

fit in Fig. 9(c). This is a significantly better fit than obtained with the physical model including the π trajectory, although still very high.

D. Summary

In this section it is seen that Model D is unable to fit the data for the reactions $\bar{p}p \rightarrow \bar{p}n\pi^+$ and $\bar{p}p \rightarrow p\bar{n}\pi^-$. The reason for this problem lies in the model and in its connections to the π trajectory. When the π trajectory is used in the calculation of the cross sections with the model, the only features of the data which are reproduced are those corresponding to strong structures and there is no way to fit the background which is present in the data. Making the unphysical assumption that the proton and neutron are identical particles, that is they possess the same charge, we are able to fit the data considerably better than before. While the best fit we get in this manner does not completely agree with the data, it still represents a great improvement over the case in which the π trajectory was used. The large average chi-square obtained from this fit represents both the high background in the data and the inability of the model to fit the data.

VI. DISCUSSION

A model in which Pomeron diagrams are added to generalized Veneziano dual diagrams was used to examine $\bar{p}p \rightarrow \bar{p}p\pi^0$, $\bar{p}n\pi^+$, and $p\bar{n}\pi^-$. Three different models for the neutral pion final state were formed:

a best theoretical model containing one free parameter, and two models each containing three free parameters in which a kinematical spin factor was either included or not included. We are able to fit the data for this reaction very well with all three of these models, with the best fit obtained with the model not containing a kinematical spin factor.

The two charged final states of this reaction are examined using one model which contains three free parameters and does not include a spin factor. This model is unable to fit these data. The reason for this failure is connected with the inability of a simple, generalized dual model to correctly calculate an amplitude using the π Regge trajectory. We finally (unphysically) neglect the charge on the outgoing nucleons, calculate a cross section for these two final states with the best model we used in the neutral pion final state calculations, and obtain an improved fit for these final states.

VII. FOOTNOTES AND REFERENCES

1. G. Veneziano, Nuovo Cimento 52A, 190 (1968).
2. R. Dolen, D. Horn, and C. Schmid, Phys. Rev. 166, 1768 (1967).
3. See, e.g., F. E. Paige, Phys. Rev. D 2, 922 (1970).
4. See, e.g., K. P. Pretzl and K. Igl, Nuovo Cimento 63A, 609 (1969).
5. K. Bardakci and H. Ruegg, Phys. Letters 28B, 324 (1968).
6. See, e.g., N. A. Törnqvist, Nucl. Phys. B18, 530 (1970).
7. M. Jacob, Lectures on Elementary Particles and Quantum Field Theory (M.I.T. Press, Cambridge, 1970); H. Harari, in Summer School in Elementary Particle Physics, Brookhaven National Laboratory, 1969, edited by R. F. Peierls (Upton, New York, 1970).
8. S. Pokorski and H. Satz, Nucl. Phys. B19, 113 (1970).
9. G. F. Chew, M. L. Goldberger, F. E. Low, and Y. Nambu, Phys. Rev. 106, 1337 (1957).
10. We assume that the Pomeron trajectory has $J^{PG} = 0^{++}$.
11. B. Diu and M. LeBellac, Nuovo Cimento 53A, 158 (1968).
12. We have investigated numerically the contribution of A' to the total amplitude and have found it to be small relative to A.
13. K. Huang, in Summer School in Elementary Particle Physics, Brookhaven National Laboratory, 1969, edited by R. F. Peierls (Upton, New York, 1970).
14. Chan Hong-Mo, R. O. Raito, G. H. Thomas, and N. A. Törnqvist, Nucl. Phys. B19, 173 (1970).

15. It should be mentioned that we have also calculated the scattering amplitude using the π and the EXD N_α - N_γ trajectories and we found these to give a very poor fit to the data.

16. Particle Data Group: N. Barash-Schmidt, A. Barbaro-Galtieri, C. Bricman, T. Lasinski, A. Rittenberg, M. Roos, A. H. Rosenfeld, P. Söding, T. G. Trippe, C. G. Wohl, Rev. Mod. Phys. 43, S1 (1971).

17. We assume that the Pomeron-p-p and Pomeron-$\bar{p}$-$\bar{p}$ vertex functions are the same.

18. E. L. Berger and G. C. Fox, Phys. Rev. 188, 2120 (1969).

19. The parameterization of the phase space factor by an exponential of slope -12 $(GeV/c)^{-2}$ is not valid for all small values of -t but in fact depends strongly upon the value of b in Eq. (10). This is so since we are combating a decreasing exponential with a rising, but not exponential, phase space, and hence the slope in Eq. (11) is determined by the cross-over point. We have numerically examined this problem and find that the values which agree with elastic scattering data are b = 18 $(GeV/c)^{-2}$ and a slope in Eq. (11) of -12 $(GeV/c)^{-2}$. [The value b = 6 $(GeV/c)^{-2}$ produced an effective slope of near 2 $(GeV/c)^{-2}$ in our theory, not the -6 $(GeV/c)^{-2}$ one should get from Eq. (11).]

20. B. Petersson and N. A. Törnqvist, Nucl. Phys. B13, 629 (1969).

21. K. Kajantie, in Proceedings of the 1970 CERN School of Physics, (CERN, Geneva, 1971).

22. J. L. Hopkinson and E. Plahte, Phys. Letters 28B, 489 (1969).

23. D. G. Scranton and E. F. Manchester, USAEC Report IS-2305. Available from Nat. Tech. Inf. Service, U.S. Department of Commerce, Springfield, Virginia 22151 (unpublished).

24. These data are the preliminary results of a $\bar{p}p$ experiment at 2.88 GeV/c using the 31-in. hydrogen bubble chamber at the Brookhaven National Laboratory. The data are being prepared for publication by H. B. Crawley et al. Previous studies of $\bar{p}p$ production reactions include W. J. Kernan, H. B. Crawley, R. A. Jespersen, and R. A. Leacock, Phys. Rev. D 1, 48 (1970); R. A. Jespersen, W. J. Kernan, and R. A. Leacock, Phys. Rev. D 1, 2483 (1970).

25. In principle the solution to this ambiguity is to form the five-dimensional equivalent of a Dalitz plot and compare that to the data, but this method is impossible because of the statistics.

26. We have only one Pomeron diagram and three dual diagrams as we consider the two Pomeron diagrams and the dual diagrams $B_5(1)$ and $B_5(1')$ to be each a single diagram which is symmetric under charge conjugation. We always treat these four diagrams in pairs.

27. We mention the fact that the pronounced dip which occurs in histogram number 4 is due entirely to the fact that we have taken the square root of t around zero and this has the effect of producing such a dip. What we have done for this histogram is as follows: for $t > 0$, we plot $\sqrt{t}$ and for $t < 0$, we use $-\sqrt{-t}$. We do this in order to avoid folding the two halves onto each other. The reason we have used the square roots of the t's is so that we may have a less sharply peaked distribution which enables us to perform the fitting procedure more accurately.

28. K. Gottfried and J. D. Jackson, Nuovo Cimento 33, 309 (1964).

29. S. B. Treiman and C. N. Yang, Phys. Rev. Letters 8, 140 (1962).

30. Specifically, the problem incurred in calculating a dual amplitude with the π trajectory is due to the fact that its first recurrence,

the pion, is both small mass and spin zero. Because it has zero spin, it will take the form $(0 + 0.02 - 0.9t)$ inside the B_5 amplitude. Since this amplitude has roughly the properties of a gamma function, and since t can get close to zero, the value of the B_5 can get very large for small values of -t. If either the π trajectory's first recurrence were not spin zero, or its mass and hence its intercept at m = 0 were greater in magnitude, the problem inherent with the trajectory would not occur. Thus the reason that the "background" structure of diagram $B_5(3)$ of Fig. 2(c) is not present in the theory of diagram $B_5(1')$ of Fig. 8(b) is because the π trajectory has produced a large pole-like structure which sits on top of the smooth background obtained from the ω trajectory. This occurrence can be seen by examining the relative sizes of the Pomeron and dual terms for the two final states. While in $\bar{p}p\pi^o$ the dual terms were $\sim 10^{-3}$ smaller than the Pomeron terms, they are approximately equal in the $\bar{p}n\pi^+$ final state calculations.

Table I. Parameter and chi-square values for Model B of the reaction $\bar{p}p \rightarrow \bar{p}p\pi^{o}$.

D_1	D_2	D_3	D	R	average chi-square
1/4	1/4	1/2	$7.8(10)^{-4}$	1.23	94.1
1/4	1/4	3/4	$9.4(10)^{-4}$	1.23	90.5
1/4	1/2	3/4	$9.4(10)^{-4}$	0.99	94.9
1/4	1/2	1	$1.3(10)^{-3}$	1.23	91.3
1/4	3/4	1	$1.2(10)^{-3}$	0.99	95.0
1/2	1/4	3/4	$1.2(10)^{-3}$	1.23	93.1
1/2	0	1/2	$8.1(10)^{-4}$	1.23	91.9

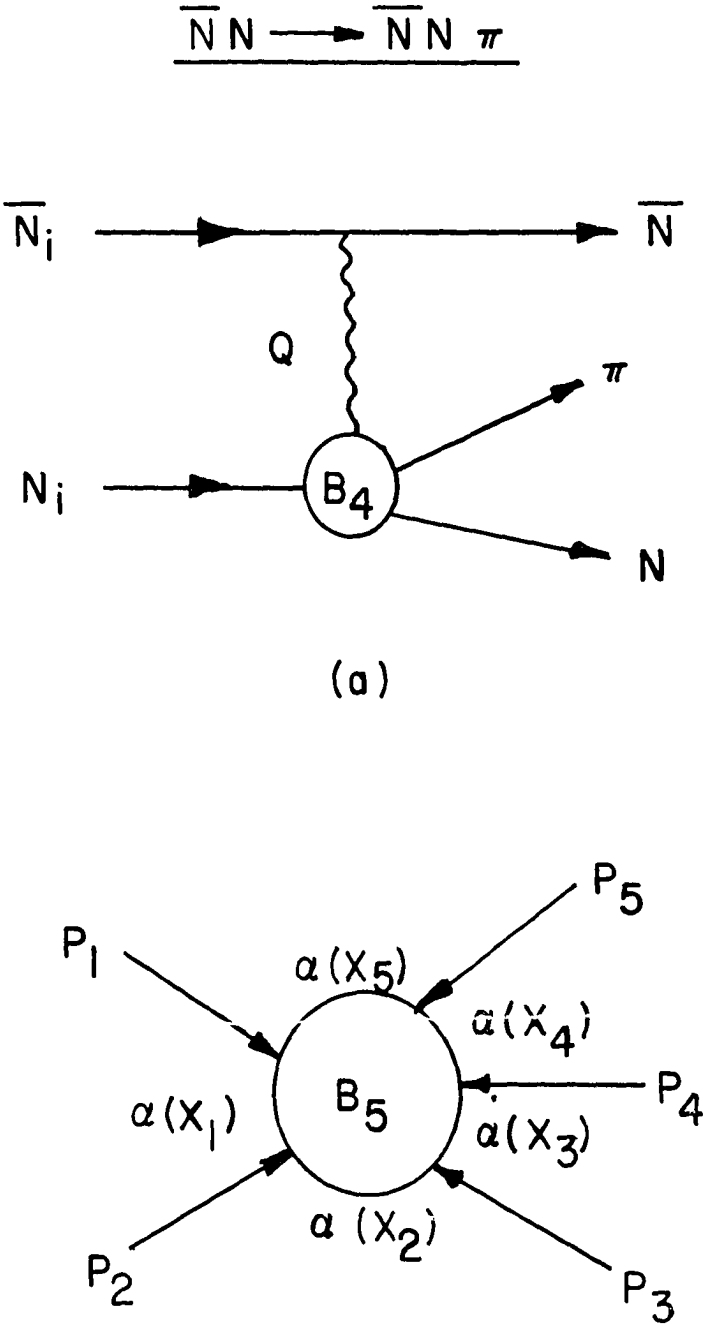

Fig. 1. (a) Pomeron exchange diagrams for the reaction $\bar{N}N \to \bar{N}N\pi$.
(b) Generalized dual diagrams for the reaction $\bar{N}N \to \bar{N}N\pi$.

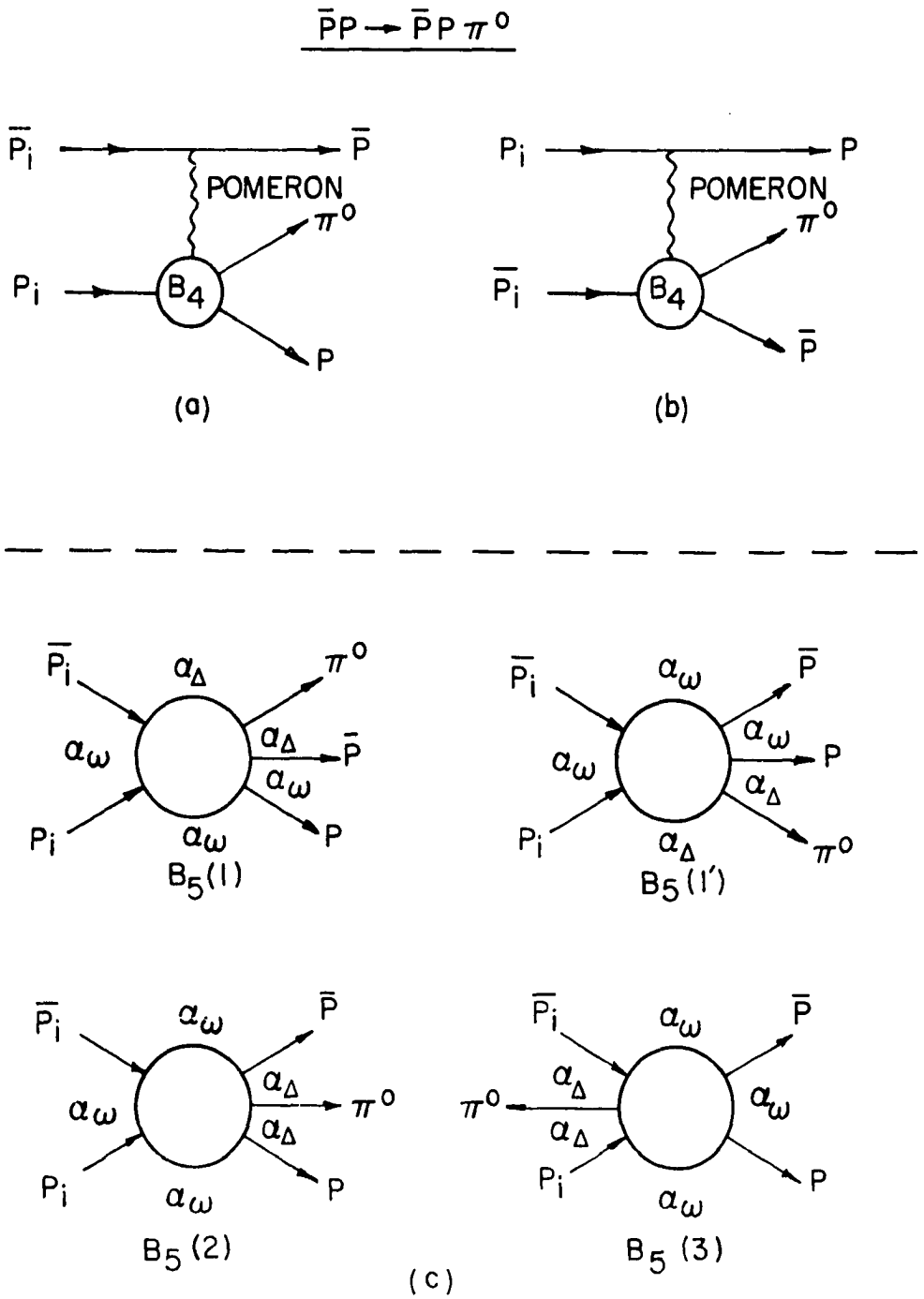

Fig. 2. (a) and (b) Two specific Pomeron diagrams for the reaction $\bar{p}p \to \bar{p}p\pi^0$. (c) The four relevant dual diagrams for the reaction $\bar{p}p \to \bar{p}p\pi^0$. The trajectory coupling to each channel is denoted between adjacent lines. Labels below each diagram are explained in the text.

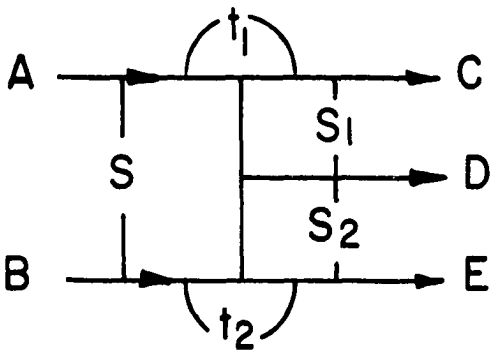

Fig. 3. Diagram showing one possible set of invariants for a three-body reaction.

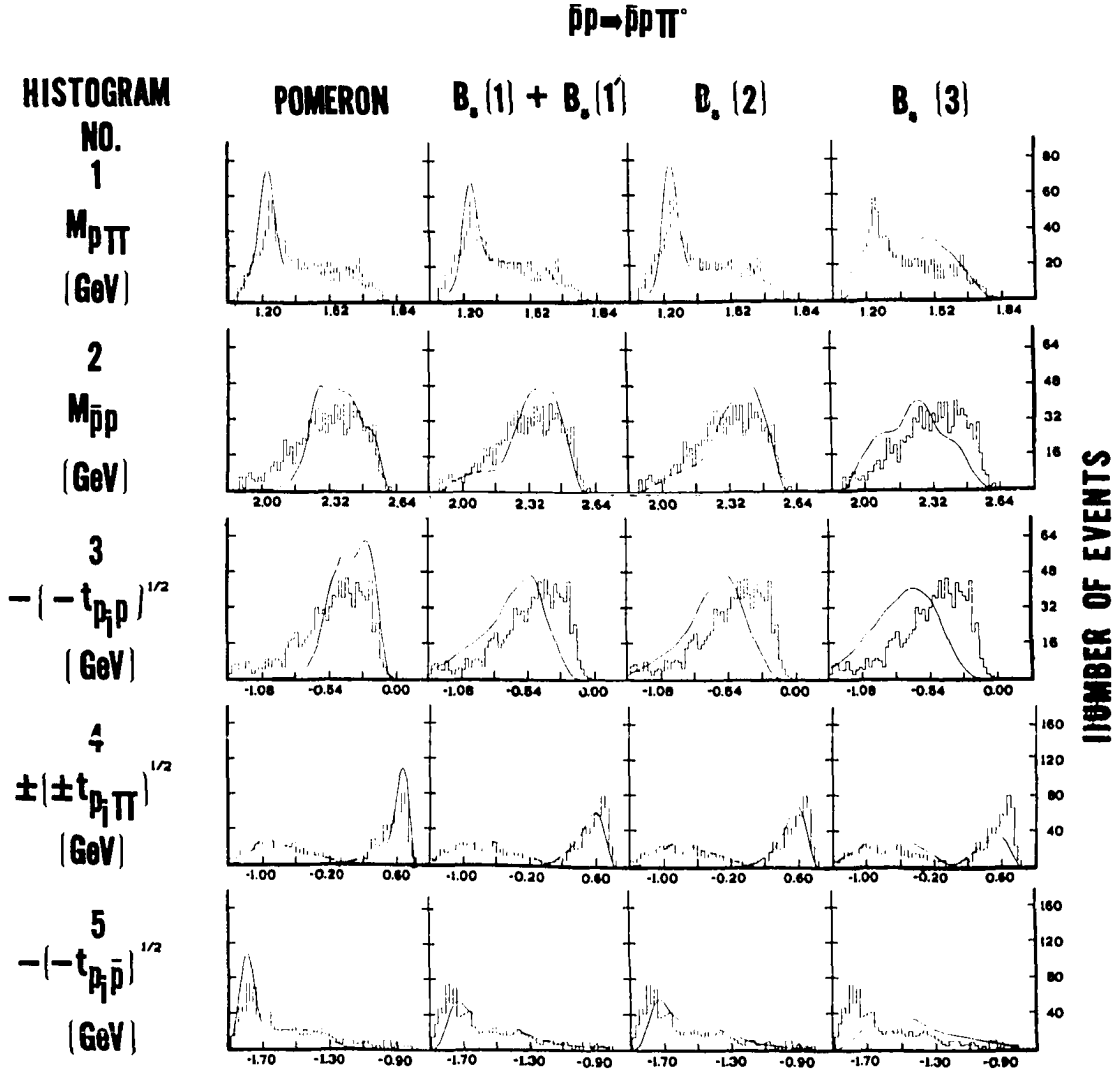

Fig. 4. Experimental histograms and theoretical predictions (smooth curves) for each of the diagrams contributing to the reaction $\bar{p}p \rightarrow \bar{p}p\pi^o$ at 2.9 GeV/c. The invariants displayed are discussed in the text and in Ref. 27.

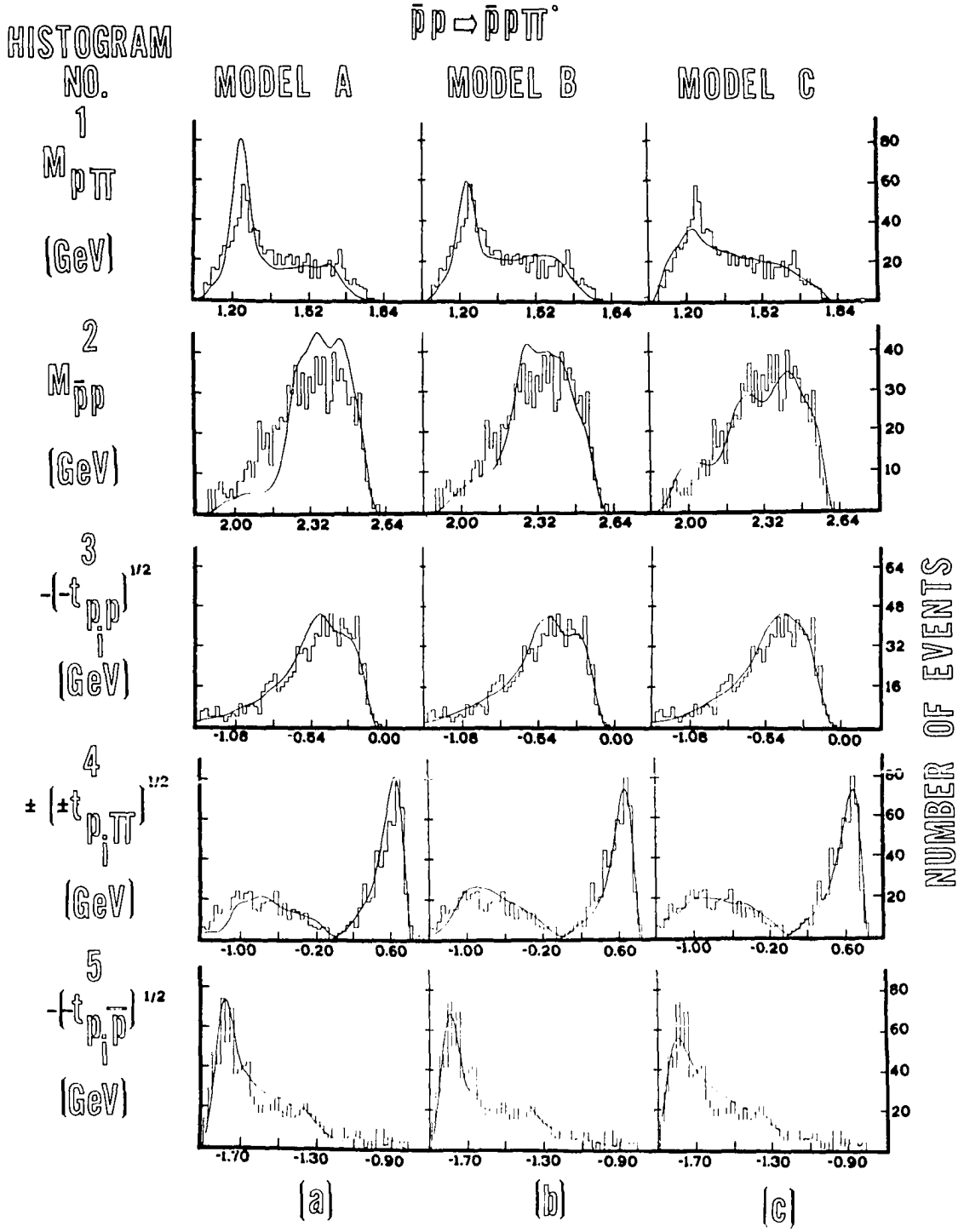

Fig. 5. (a), (b), and (c) Experimental histograms and theoretical predictions (smooth curves) for the best fits of Models A, B, and C, respectively, to the reaction $\bar{p}p \rightarrow \bar{p}p\pi^{o}$ at 2.9 GeV/c.

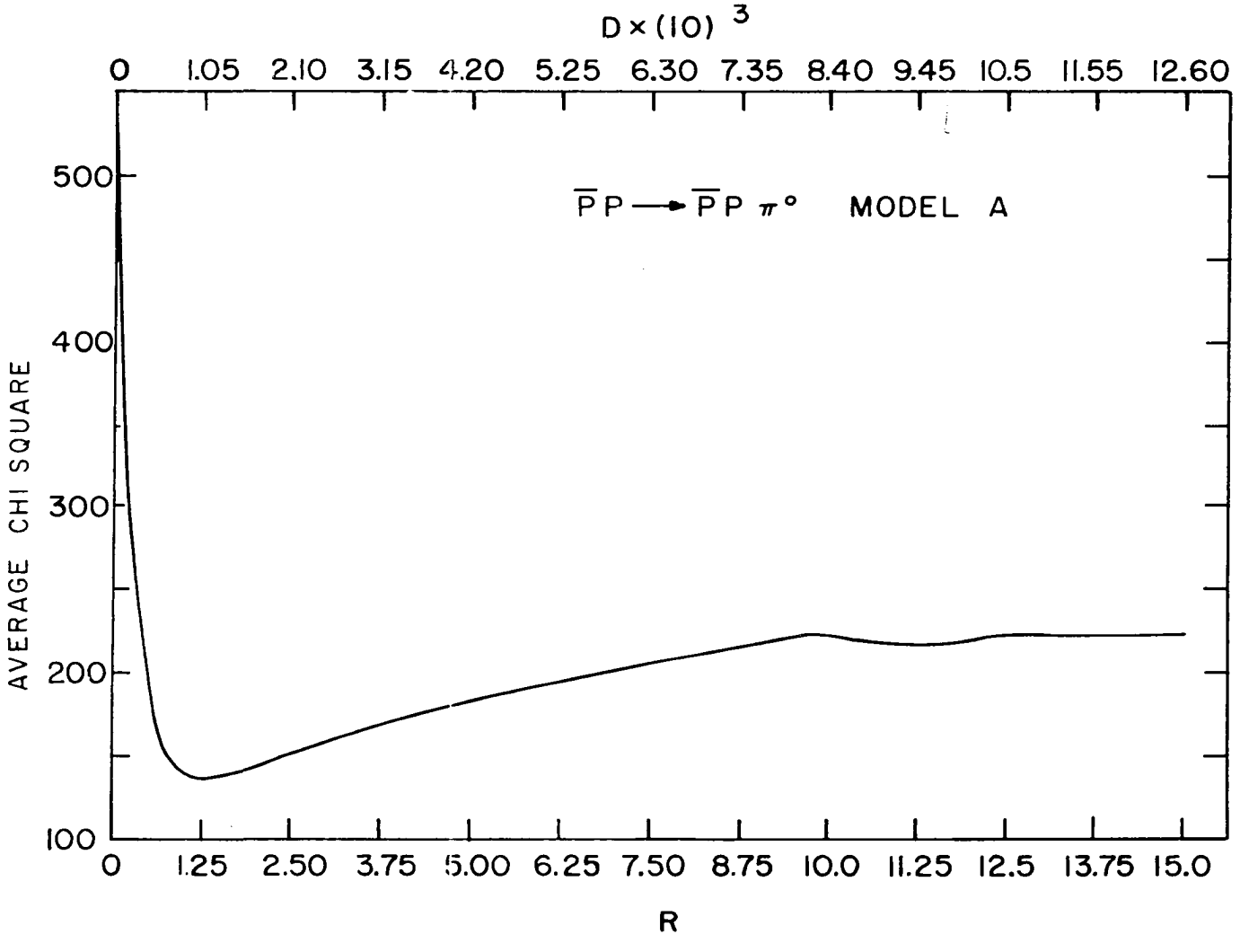

Fig. 6. Plot of the chi-square function for Model A of the reaction $\bar{p}p \rightarrow \bar{p}p\pi^{o}$ as a function of the parameter D [see Eq. (14) of text].

$\bar{p}p \rightarrow \bar{p}p\pi^{\circ}$

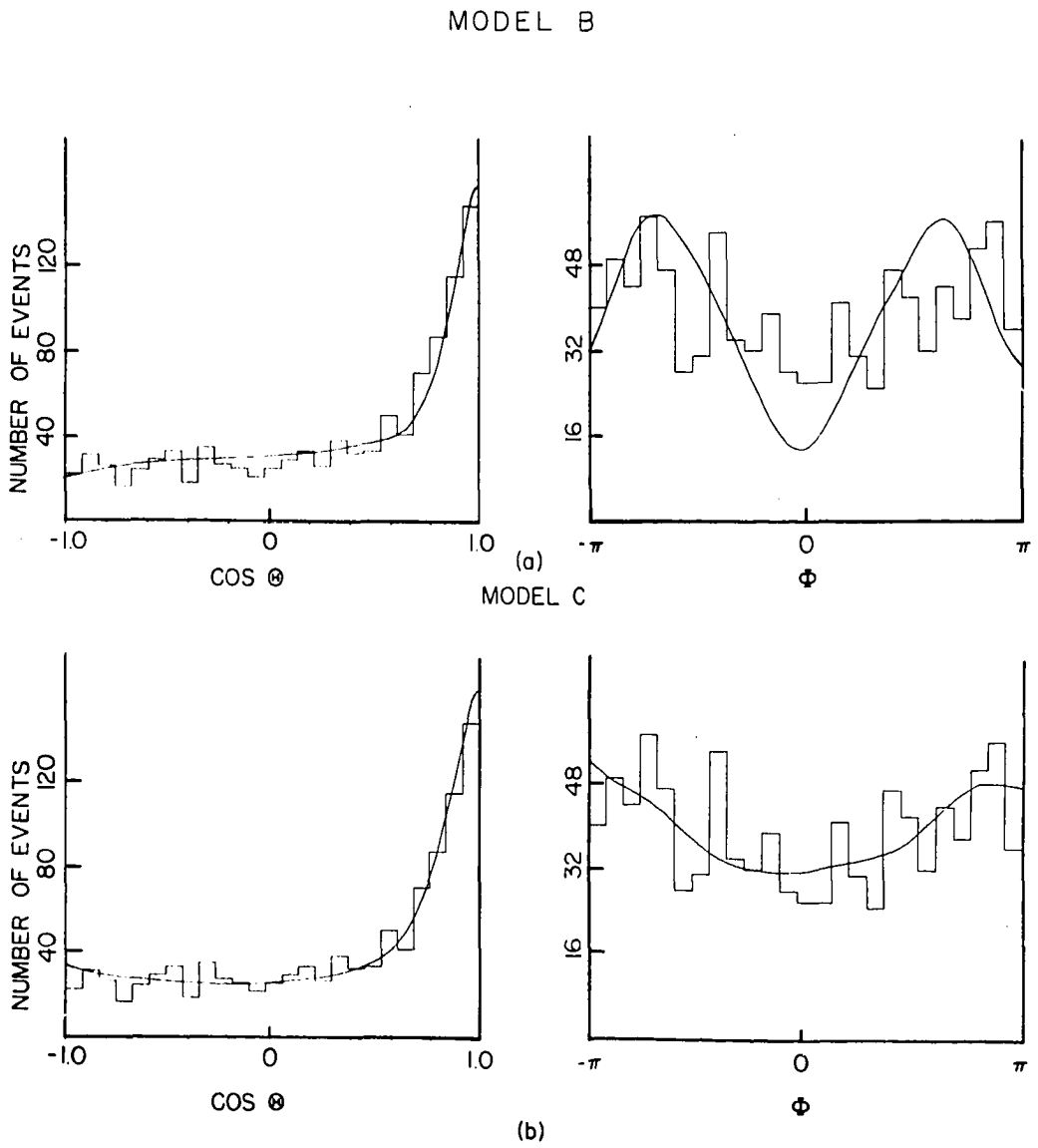

Fig. 7. (a) Experimental histograms and theoretical predictions (Model B) for the Jackson angle θ and Treiman-Yang angle φ calculated in the rest frame of the outgoing $\pi^{o}p$ system for the reaction $\bar{p}p \rightarrow \bar{p}p\pi^{o}$.
(b) Identical distributions for Model C for reaction $\bar{p}p \rightarrow \bar{p}p\pi^{o}$.

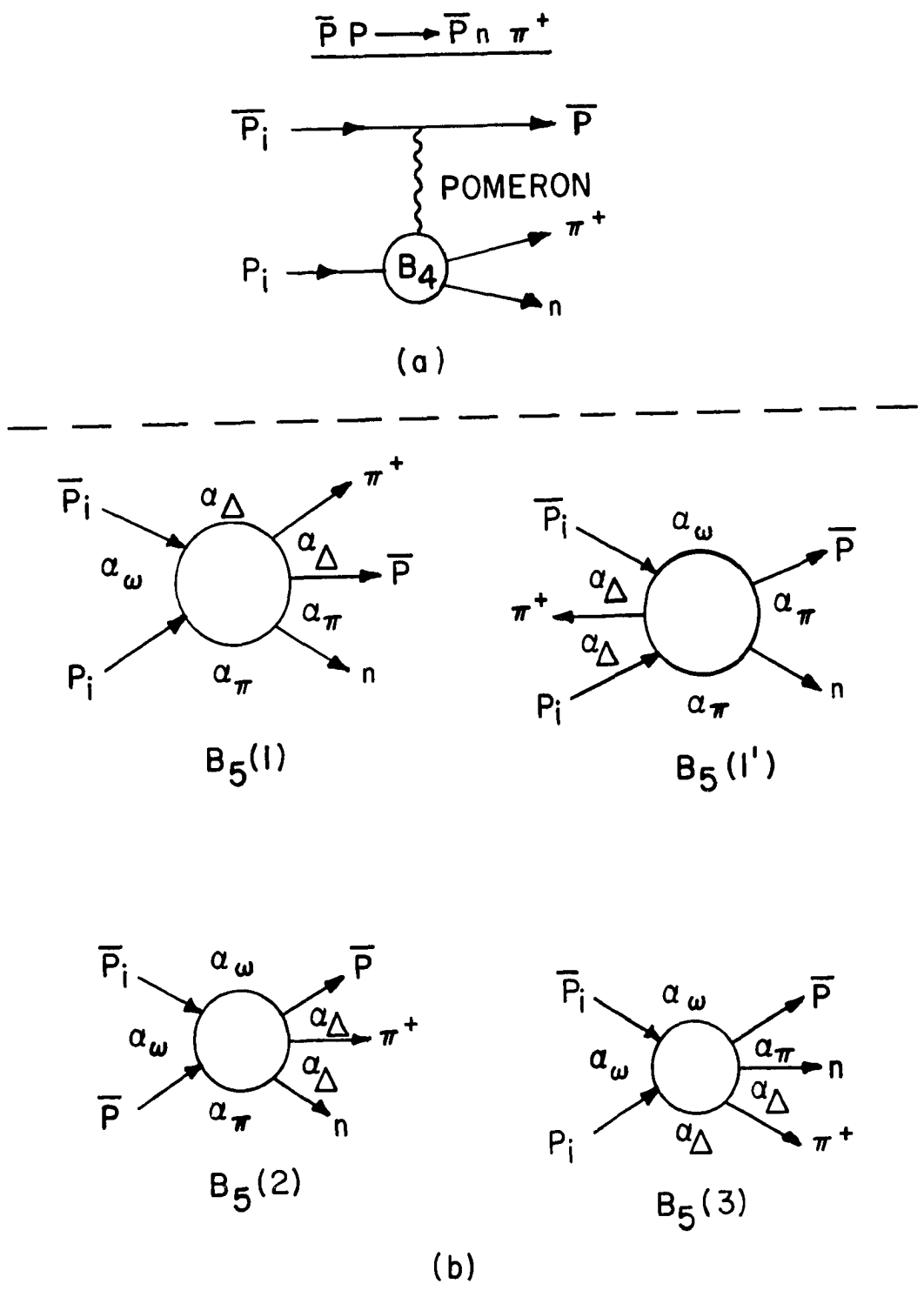

Fig. 8. (a) Pomeron exchange diagram for the reaction $\bar{p}p \to \bar{p}n\pi^+$.
(b) The four relevant dual diagrams for the reaction $\bar{p}p \to \bar{p}n\pi^+$. The trajectory coupling to each channel is denoted between adjacent lines. Labels below each diagram are explained in the text.

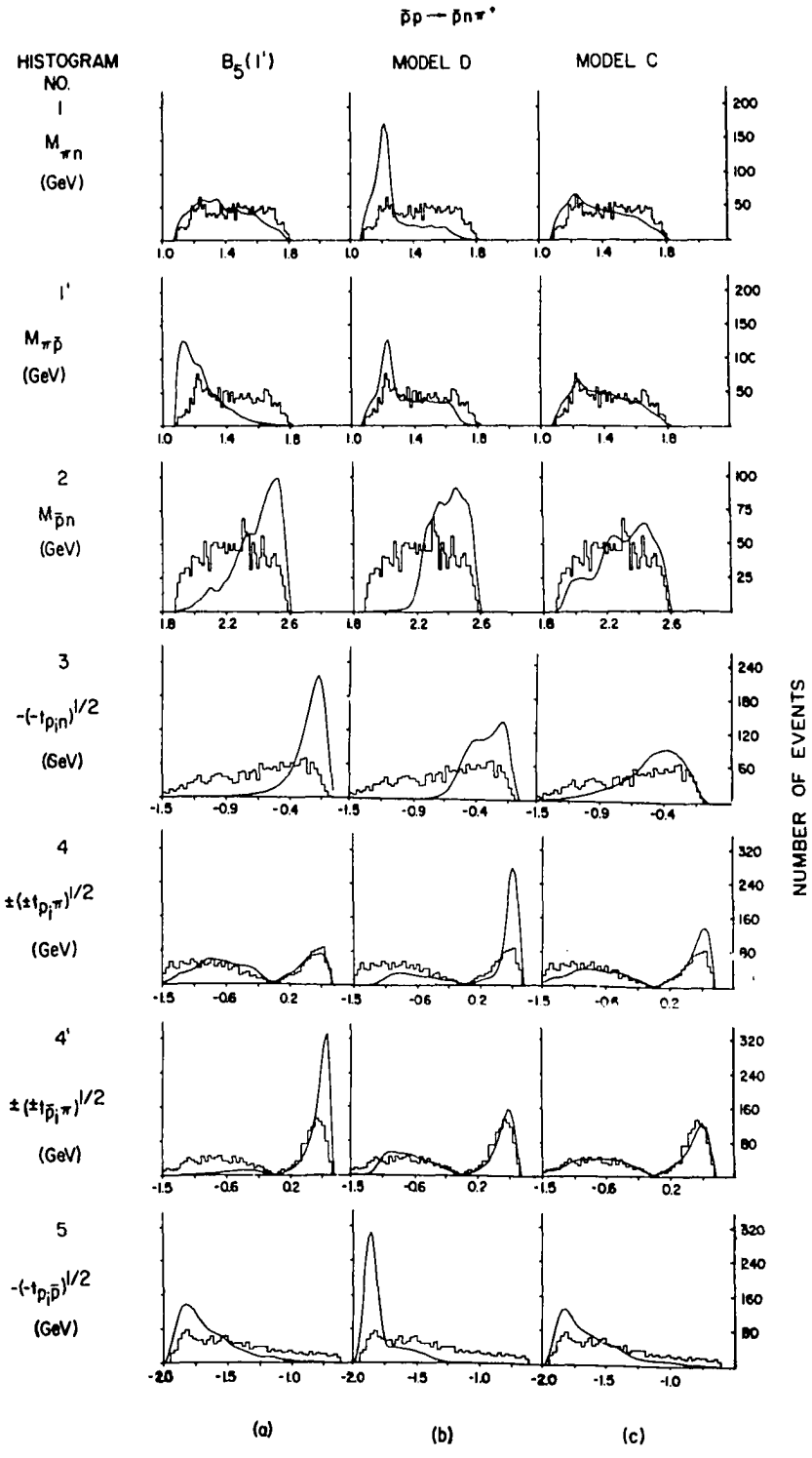

Fig. 9. (a) Experimental histograms and theoretical predictions (smooth curves) for the diagram $B_5(1')$ for the reaction $\bar{p}p \to \bar{p}n\pi^+$ (see text). (b) and (c) Experimental histograms and theoretical prections for the best fits of Models D and C respectively to the reaction $\bar{p}p \to \bar{p}n\pi^+$ at 2.9 GeV/c.

VIII. ACKNOWLEDGMENTS

The author wishes to thank Professors R. A. Leacock and H. B. Crawley for their help and advice during the course of this work, and also to thank the Iowa State University-Ames Laboratory Bubble Chamber Group for allowing the use of their unpublished data.